nature chemical engineering

Supplementary information

https://doi.org/10.1038/s44286-024-00076-8

Kilowatt-scale tandem CO_2 electrolysis for enhanced acetate and ethylene production

In the format provided by the authors and unedited

Table of Contents

Supplementary Discussion 1: Techno-economic Analysis

The techno-economic simulation of tandem CO_2 electrolysis to acetic acid presented in this work was performed using our previously published model.[1] This model was adjusted to incorporate the performance parameters and material usage for the kW-scale system presented in this work (Table S2). Other major assumptions made in the techno-economic model presented in this work are detailed in Table S3. The techno-economic model encapsulated both the tandem CO_2 electrolysis system as well as downstream separations. The final production cost of acetic acid was determined by performing a numerical evaluation of the product price needed to achieve a net present value of zero at the end of the plant life.

The downstream separations included distillation, acetate protonation to acetic acid, and recovery of the 2 M KOH electrolyte. Separation modelling was performed in ASPEN Plus software using the Economic Analyzer plugin and the NRTL-HOC property method. Glacial acetic acid (>99.5%) was produced by first protonating the potassium acetate with a HCl solution to produce acetic acid and KCl which was recovered and converted back to KOH. A liquid-liquid extraction was then performed using ethyl acetate followed by a distillation process composed of a dehydration and water purification column. Additional details of the separation modelling are outlined in our previously published work.[1] After the separations were performed, the final product was obtained as pure glacial acetic acid. The model for the cost of CO production was based upon state-of-the-art solid oxide electrolyzer cell technology as described in Table S4. The overall cost breakdown for electrochemical acetic acid production via tandem CO_2 electrolysis is presented in Table S5.

Supplementary Discussion 2: Acetate Faradaic Efficiency from Partial Ethanol Oxidation

Our previous work estimated that about 30% of the acetate produced could result from partial ethanol oxidation at relatively high current densities (600 mA cm^{-2}).[1] This "30%" was determined by comparing CO electroreduction results using an IrO_x anode that is not active towards alcohol oxidation with results obtained using a $NiFeO_x$ anode that is highly active towards alcohol oxidation. Further confirmation that about 30% of the produced acetate results from partial ethanol oxidation was obtained by quantifying the gas composition at the anode outlet. The missing oxygen Faradaic efficiency (FE) from the oxygen evolution reaction could be accounted for by the FE towards partial ethanol oxidation. Higher current densities can increase the role of ethanol oxidation due to faster crossover rates driven by larger concentration gradients. Thus, a smaller partial ethanol oxidation contribution than the 30% of acetate FE observed at 600 mA cm^{-2} is expected at the more moderate current densities used at the kW-scale in this work (100-300 mA cm^{-2}). Here, 30% serves as the upper boundary of potential FE error. It takes 4 electrons to generate 1 mol of acetic acid/acetate from CO (Equation 1) and 8 electrons to generate 1 mol of ethanol from CO (Equation 2):

$$2CO + 4e^- + 4H_2O \rightarrow CH_3COOH + 4OH^- \quad \text{(S1)}$$

$$2CO + 8e^- + 7H_2O \rightarrow CH_3CH_2OH + 8OH^- \quad \text{(S2)}$$

If 35% total acetate FE is observed with up to 30% of this 35% total acetate FE resulting from the partial oxidation of ethanol, the total FE error can be estimated below in equation 3:

$$35\%\ \text{total acetate FE} \times 30\%\ \text{from partial EtOH oxidation} \times \frac{4e^-_{AcO}}{8e^-_{EtOH}} \approx 5\% \quad \text{(S3)}$$

Thus, the FE error contribution from assuming that the acetate was produced via a 4 e^- reduction process is estimated to be ≤5%.

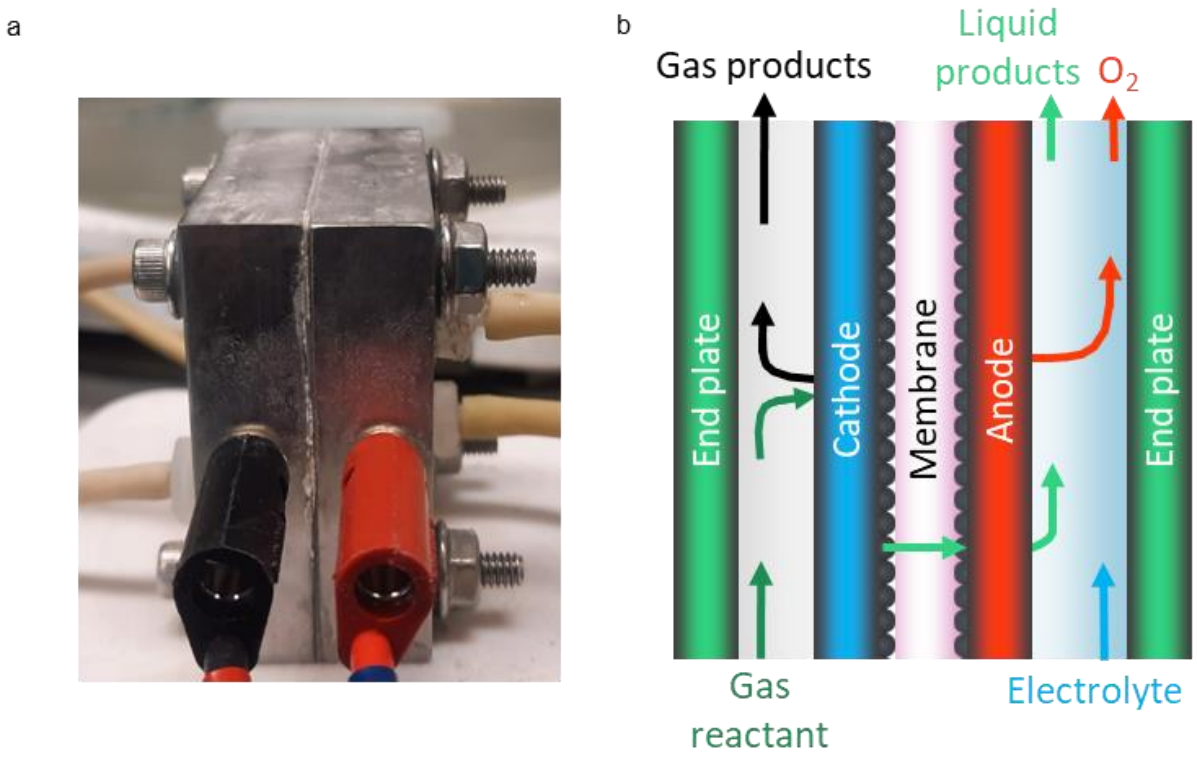

Figure S1. (a) Photograph and (b) schematic of a membrane electrode assembly (MEA) electrolyzer.

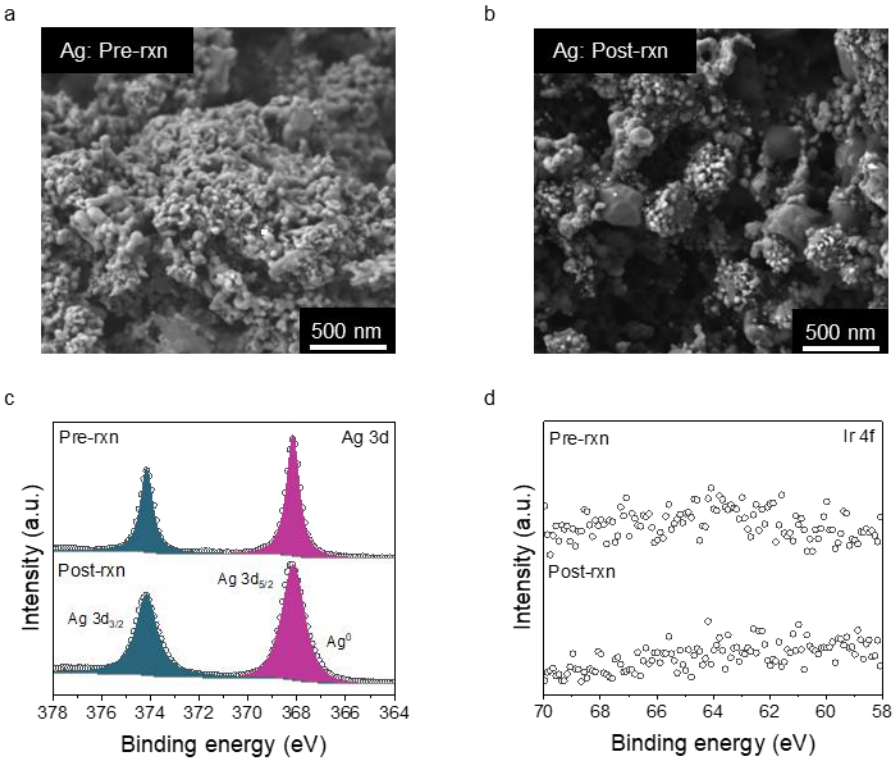

Figure S2. Characterization of Ag electrode. SEM images of (a) pre- and (b) post-reaction electrodes. (c) Ag 3d and (d) Ir 4f XPS measurements of pre- and post-reaction electrodes. Post-reaction electrode was obtained after 300 h two-step tandem CO_2 electrolysis experiment shown in Fig. 2.

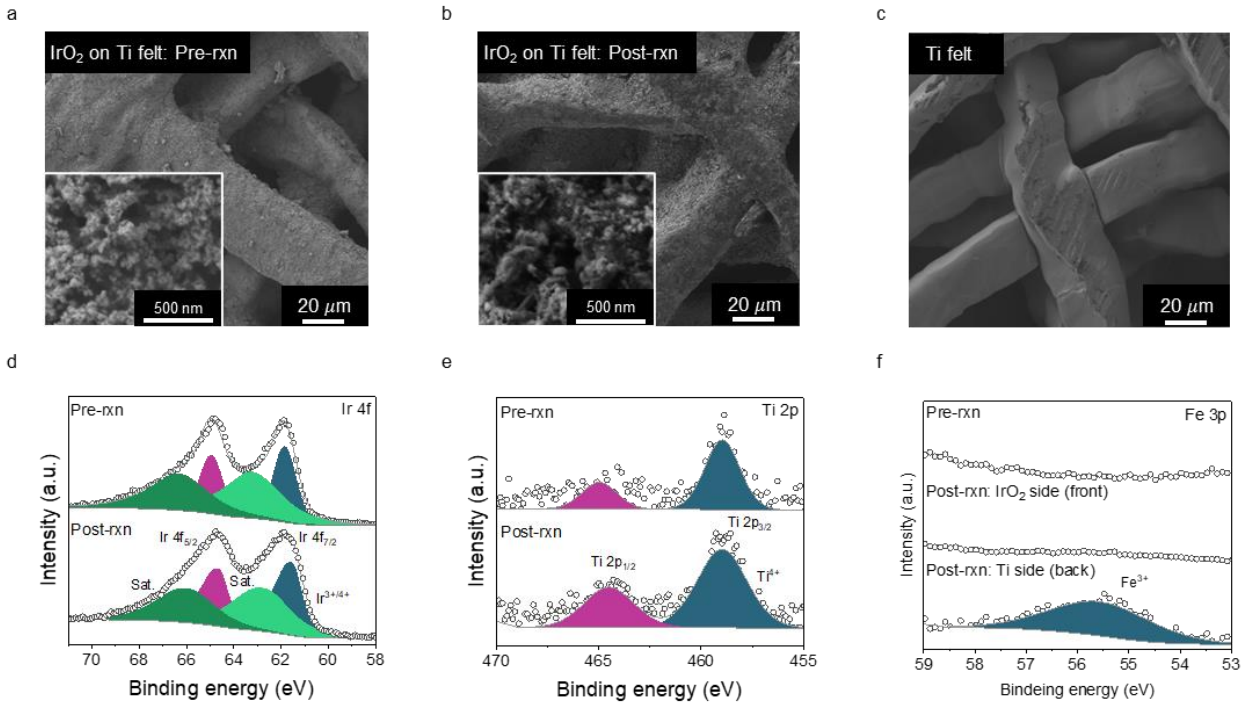

Figure S3. Characterization of IrO_2 on Ti electrode. SEM images of (a) pre- and (b) post-reaction electrode, and (c) Ti felt. (d) Ir 4f, (e) Ti 2p, and (f) Fe 3p XPS measurements of pre- and post-reaction electrodes. Post-reaction electrode was obtained after 300 h two-step tandem CO_2 electrolysis experiment shown in Fig. 2.

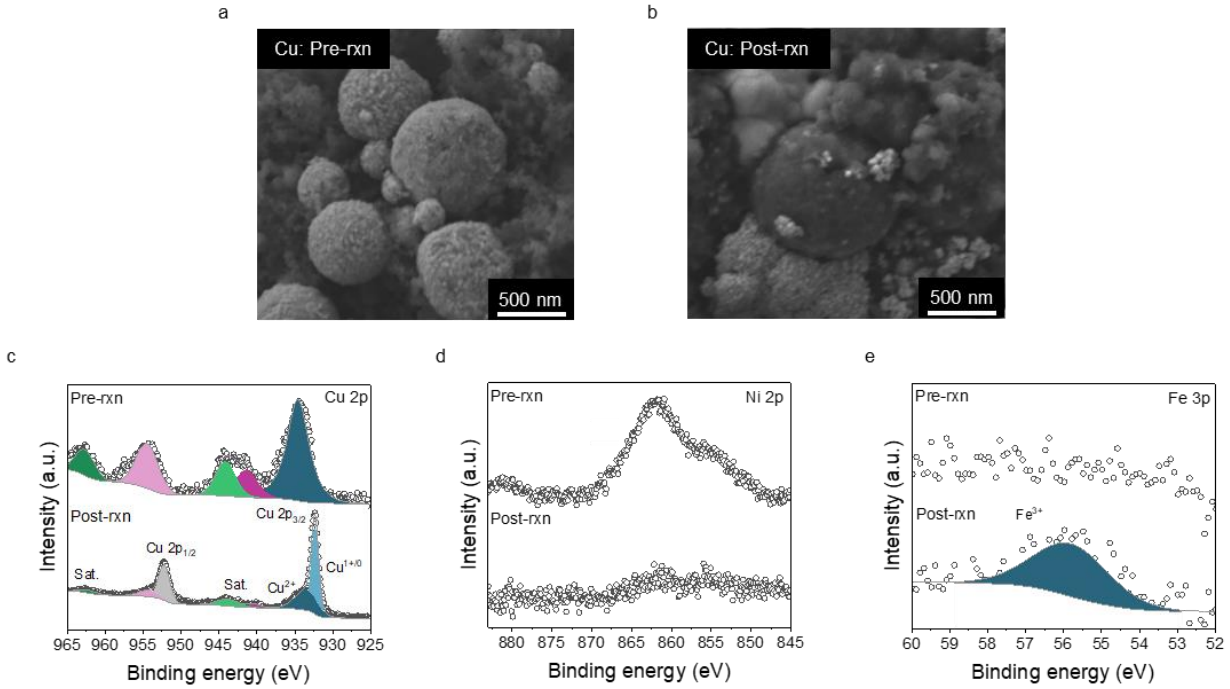

Figure S4. Characterization of Cu electrode. SEM images of (a) pre- and (b) post-reaction electrode. (c) Cu 2p, (d) Ni 2p, and (e) Fe 3p XPS measurements of pre- and post-reaction electrodes. Post-reaction electrode was obtained after 300 h two-step tandem CO_2 electrolysis experiment shown in Fig. 2.

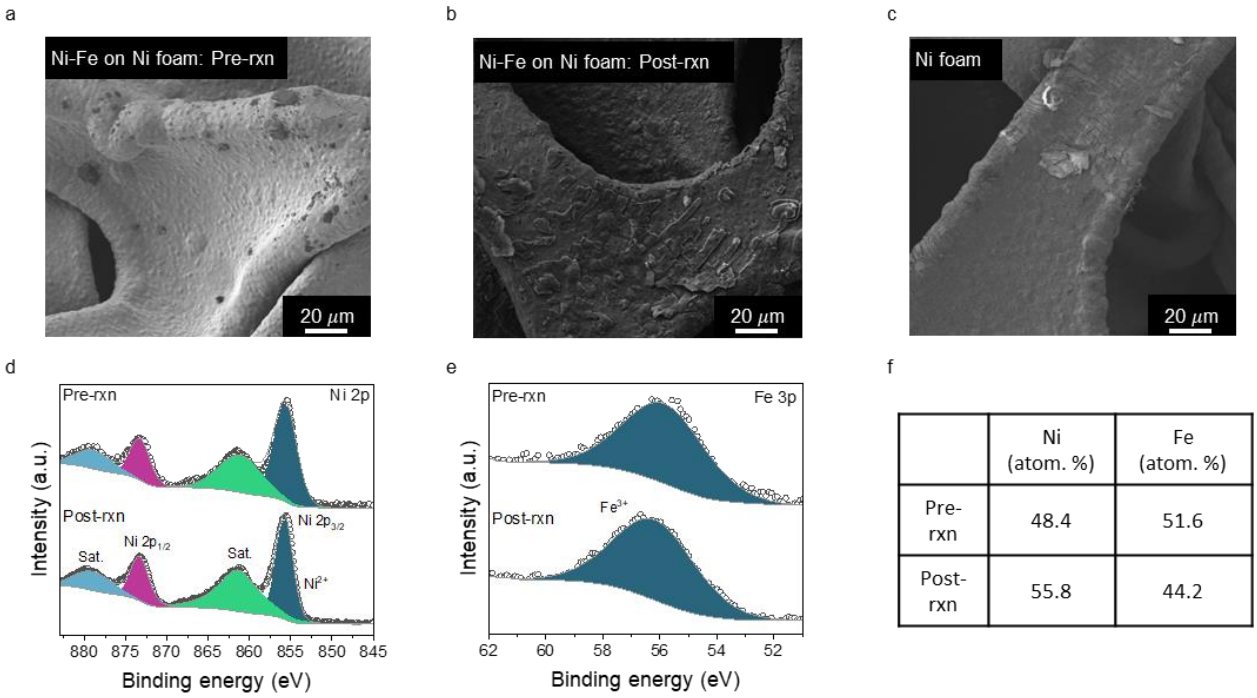

	Ni (atom. %)	Fe (atom. %)
Pre-rxn	48.4	51.6
Post-rxn	55.8	44.2

Figure S5. Characterization of Ni-Fe on Ni foam electrode. SEM images of (a) pre- and (b) post-reaction electrode, (c) and Ni foam. (c) Ni 2p and (d) Fe 3p XPS measurements of pre- and post-reaction electrodes. (f) Table of Ni and Fe ratio obtained from XPS measurements. Post-reaction electrode was obtained after 300 h two-step tandem CO_2 electrolysis experiment shown in Fig. 2.

a

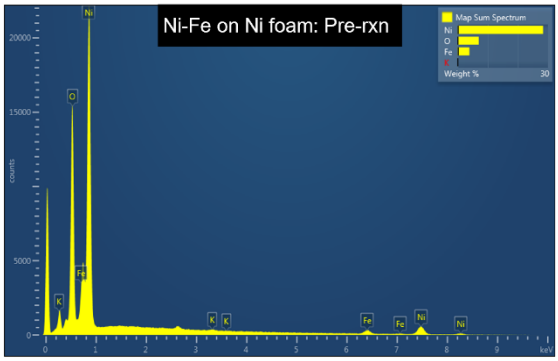

b

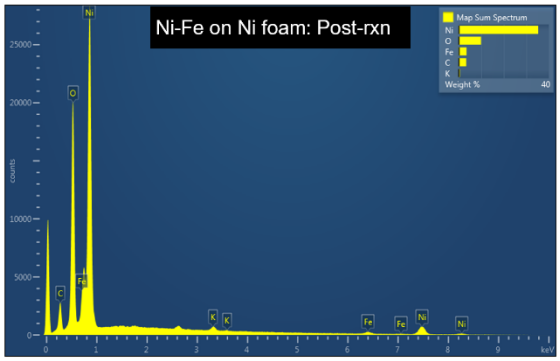

c

	Ni (atom. %)	Fe (atom. %)
Pre-rxn	86.8	13.2
Post-rxn	90.5	9.5

Figure S6. EDS measurements of (a) pre- and (b) post-reaction Ni-Fe on Ni foam electrodes. (c) Table of Ni and Fe ratio obtained from EDS measurements. Post-reaction electrode was obtained after 300 h two-step tandem CO_2 electrolysis experiment shown in Fig. 2.

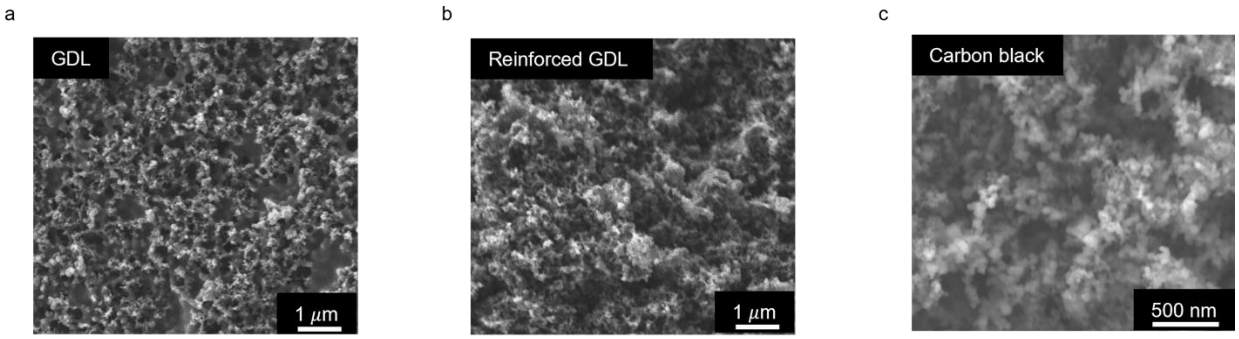

Figure S7. SEM images of (a) GDL, (b) reinforced GDL, and (c) carbon black.

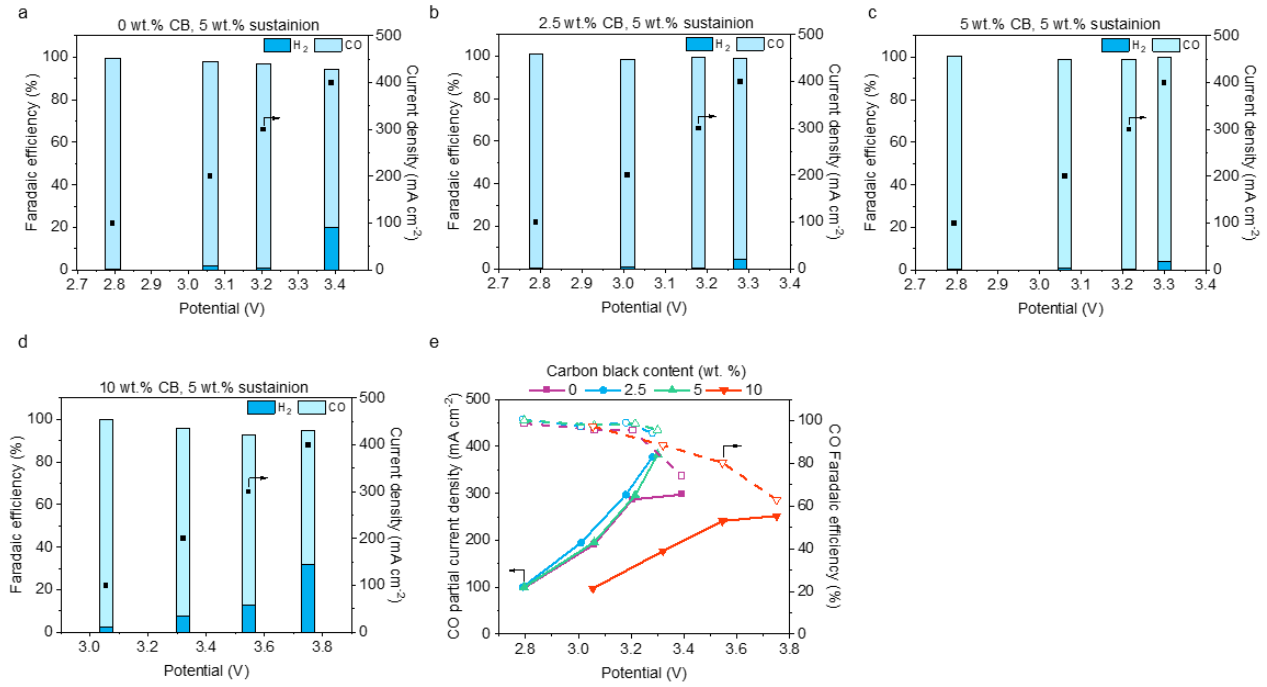

Figure S8. Faradaic efficiency and current density vs. potential for CO_2 electrolysis using Ag and 5wt. % Sustainion with (a) 0 wt. %, (b) 2.5 wt. %, (c) 5 wt.%, and (d) 10 wt.% carbon black (CB). (e) Comparison of CO_2 electrolysis using Ag with different loadings of CB. 50 mL min^{-1} CO_2 and 100 mM $CsHCO_3$ were used.

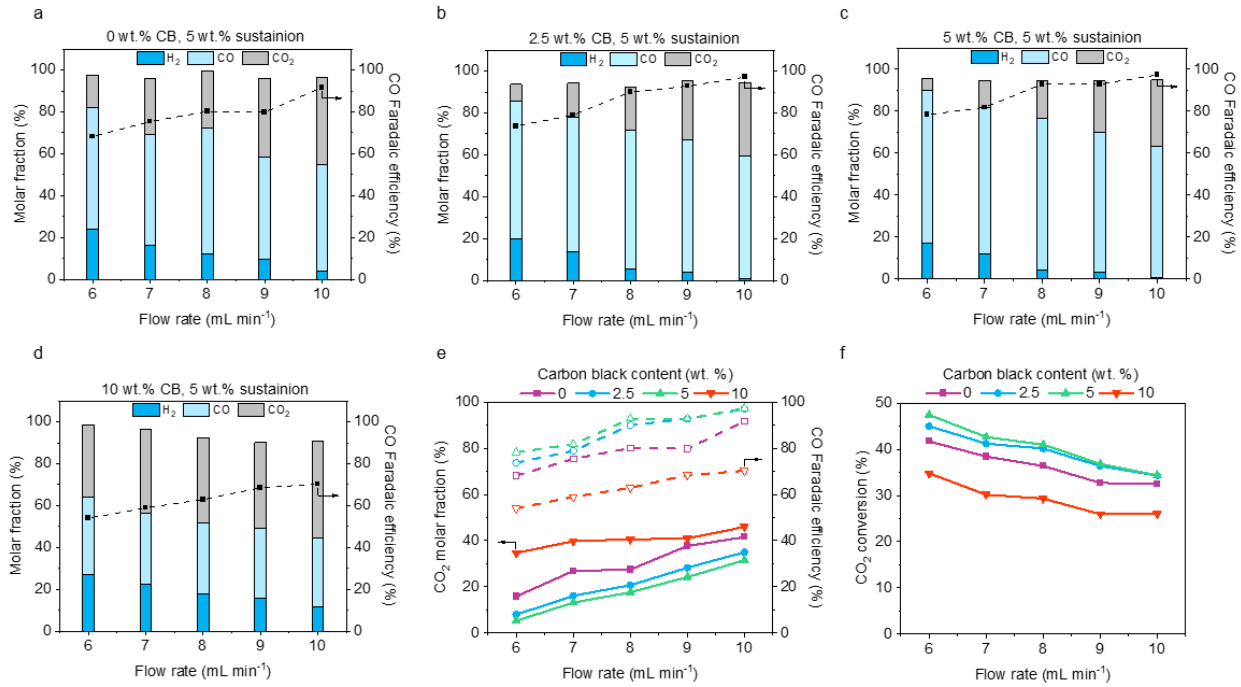

Figure S9. Gas molar fraction and CO Faradaic efficiency vs. flow rate for CO_2 electrolysis using Ag and 5wt. % Sustainion with (a) 0 wt. %, (b) 2.5 wt. %, (c) 5 wt.%, and (d) 10 wt.% carbon black (CB). Comparison of CO_2 electrolysis using Ag with different loadings of CB for (e) CO_2 molar fraction and CO Faradaic efficiency, and (f) CO_2 conversion. 100 mM $CsHCO_3$ was used as electrolyte.

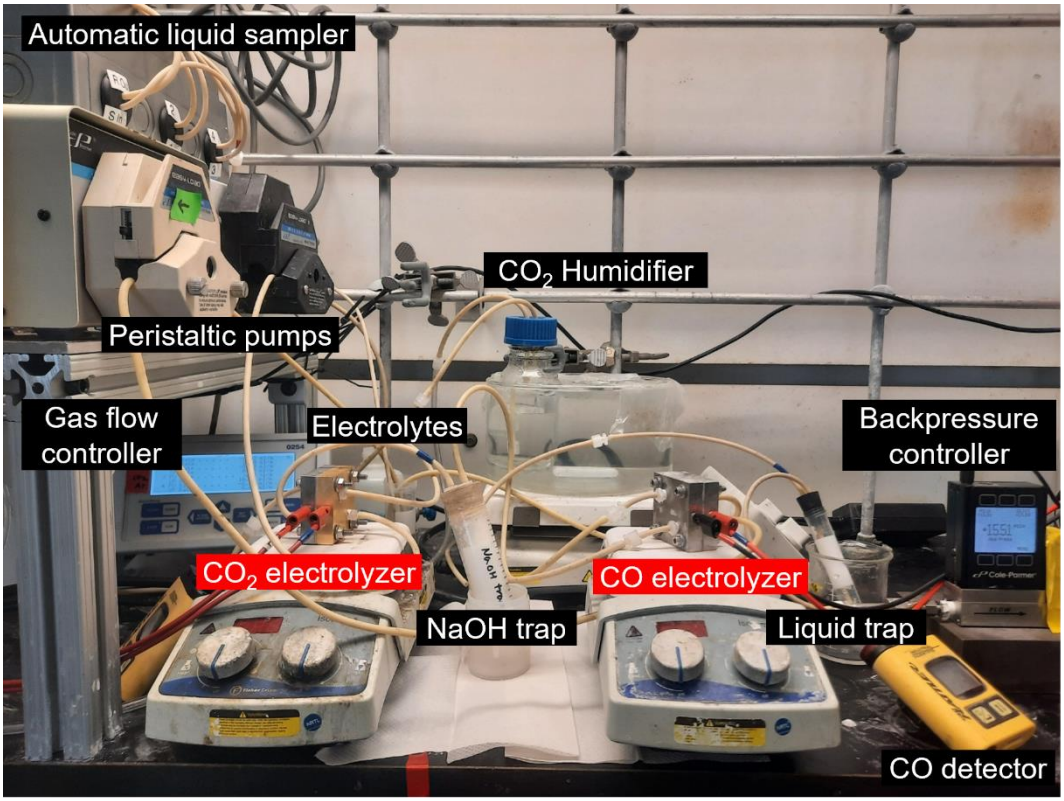

Figure S10. Photograph of a two-step tandem CO_2 electrolysis setup.

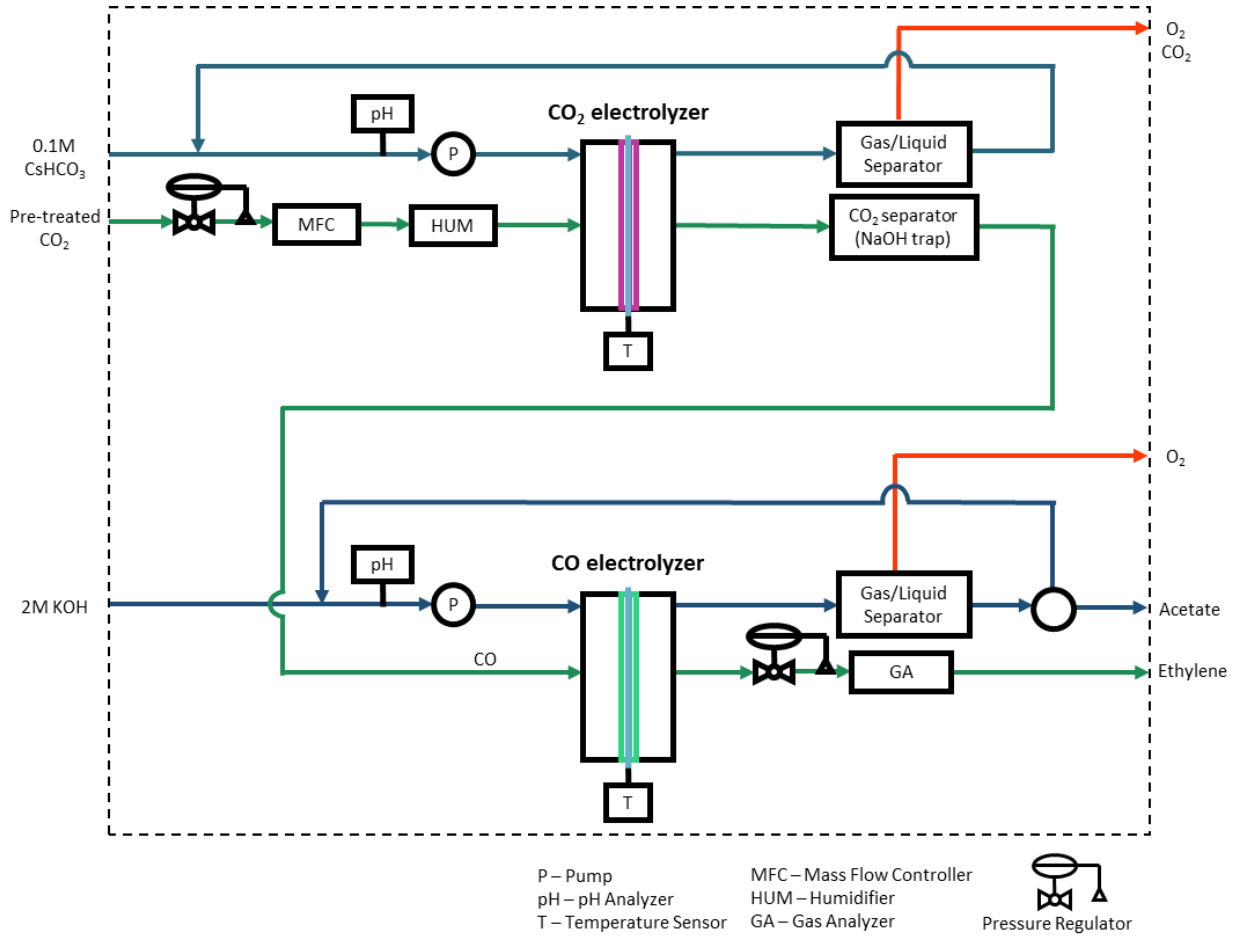

Figure S11. P&ID of a two-step tandem CO_2 electrolysis setup.

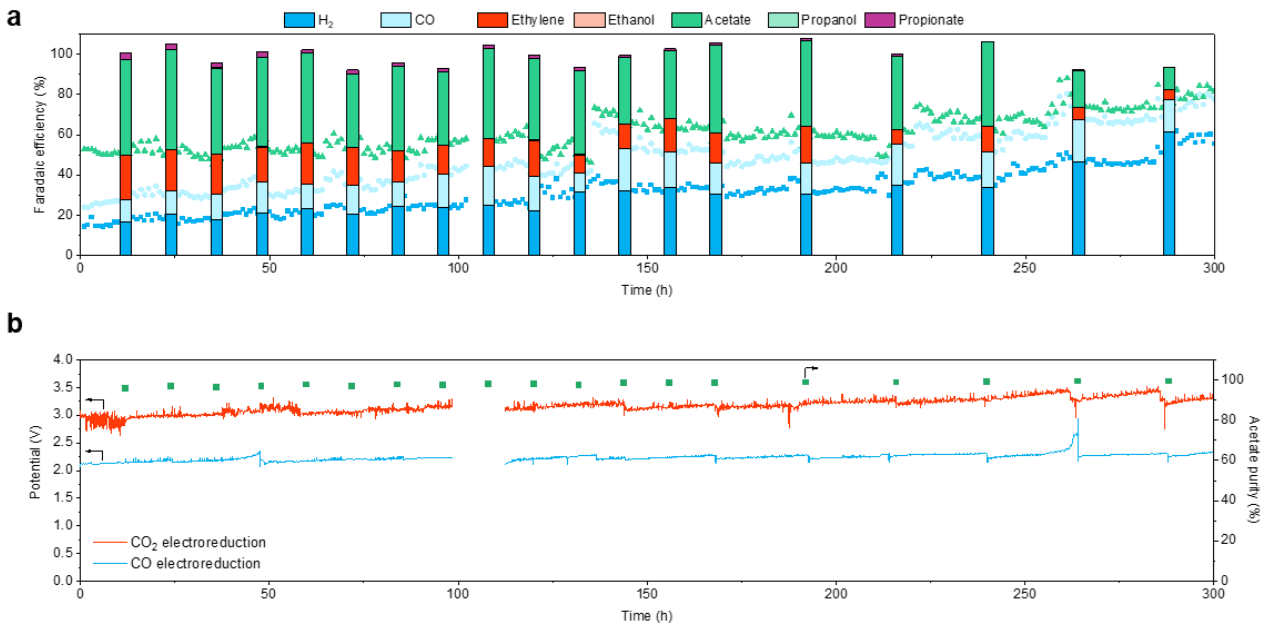

Figure S12. Integrated two-step tandem CO_2 electrolysis for 300 h. (a) Faradaic efficiency vs. time for integrated two-step tandem CO_2 electrolysis. 8 mL min^{-1} CO_2 and NaOH trap was used. For CO_2 electrolysis (100 mA cm^{-2}), $CsHCO_3$ was recirculated while for CO electrolysis (100 mA cm^{-2}), 2 M KOH was replenished every 24 h. (b) Potentials of CO_2 and CO electrolysis and acetate purity vs. time. Data lost at around 100 h was due to PC recording malfunction.

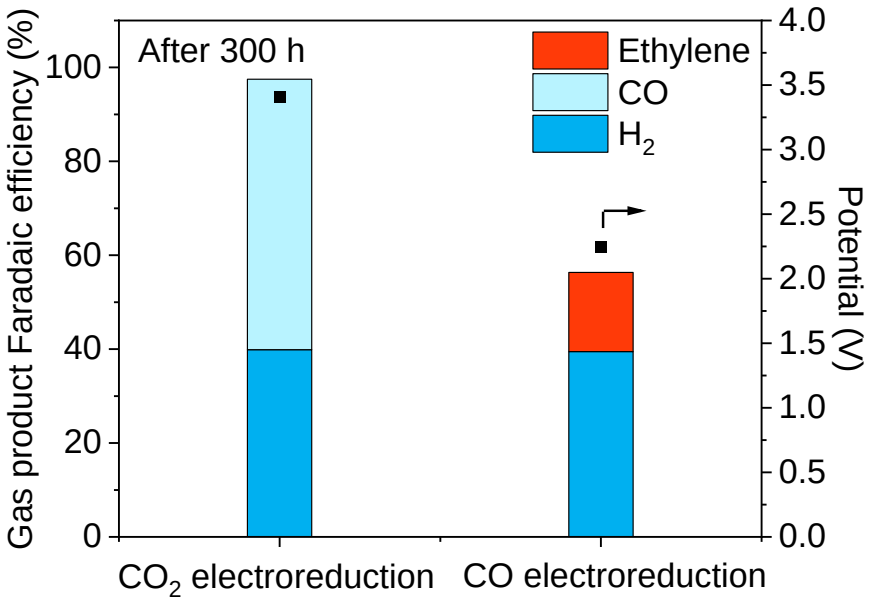

Figure S13. Gas product Faradaic efficiency and potential of CO_2 and CO electrolyzers after 300 h operation in the two-step tandem electrolysis. Highly pure CO_2 and CO were supplied to CO_2 and CO electrolyzers, respectively.

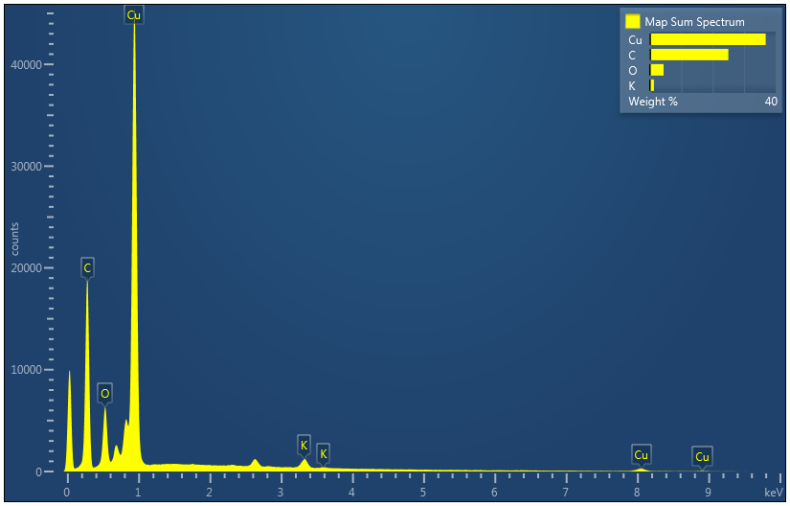

Figure S14. EDS measurement of post-reaction Cu electrode after 300 h operation in the two-step tandem electrolysis.

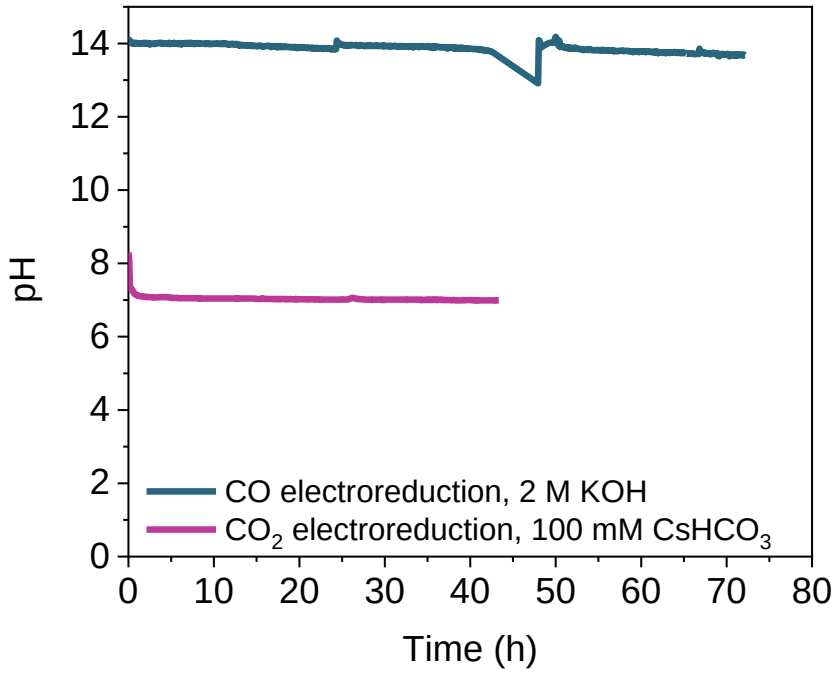

Figure S15. pH measurement of electrolytes for CO_2 and CO electrolysis at 100 mA cm^{-2}. (2 M KOH electrolyte swapped ~47 h in CO electrolysis experiment).

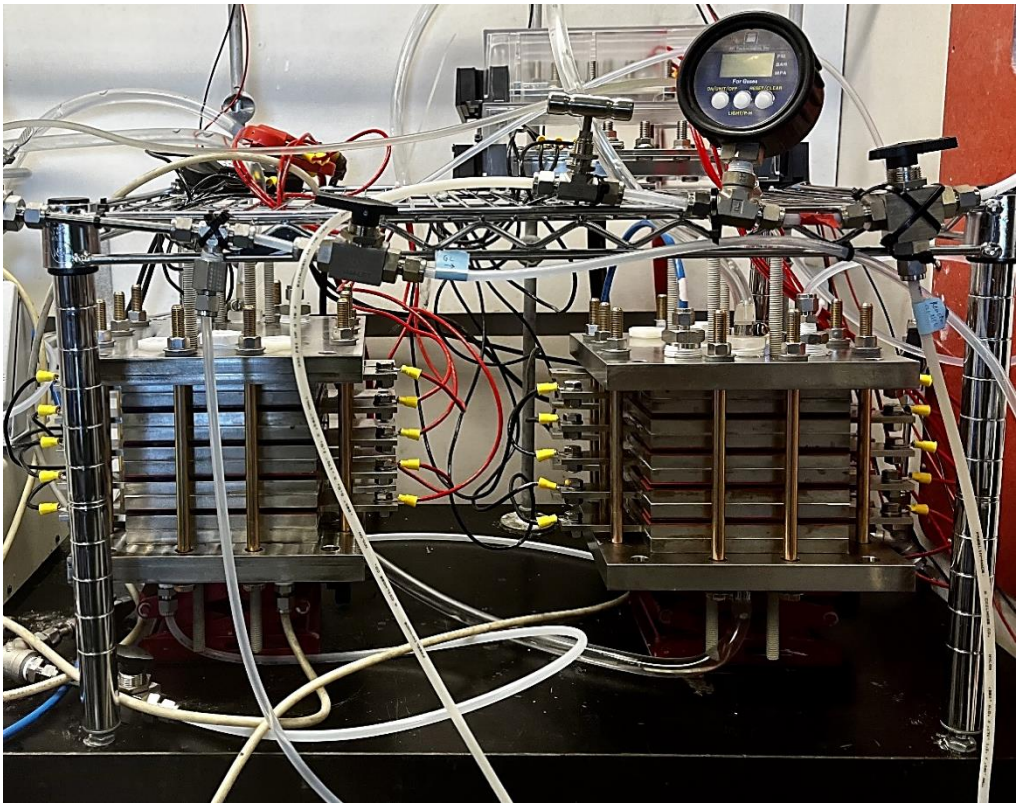

Figure S16. Photograph of 1,000 cm^2, 10 cell CO_2/CO electrolyzer stacks.

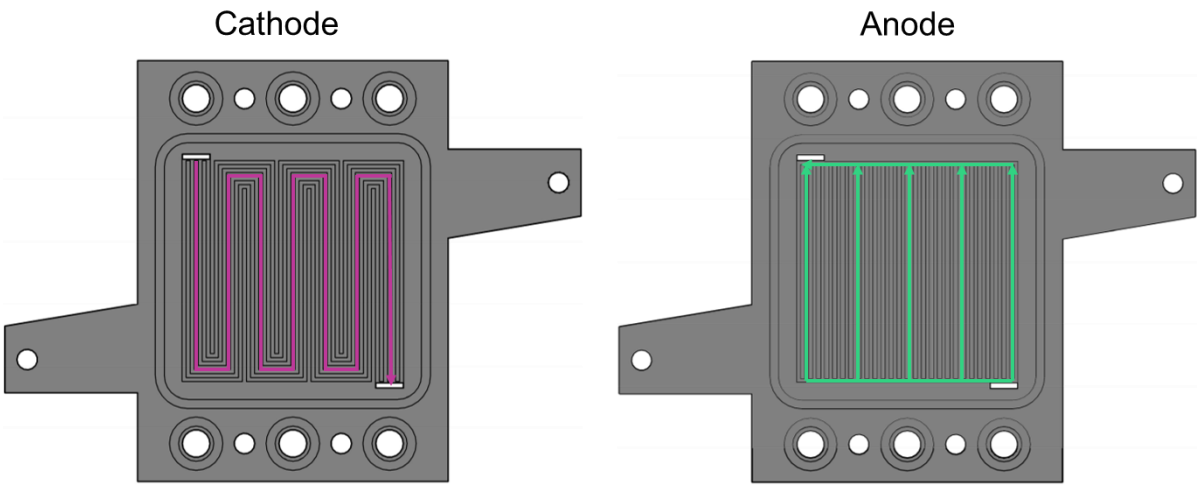

Figure S17. Cathode flow field design (left) and anode flow field design (right).

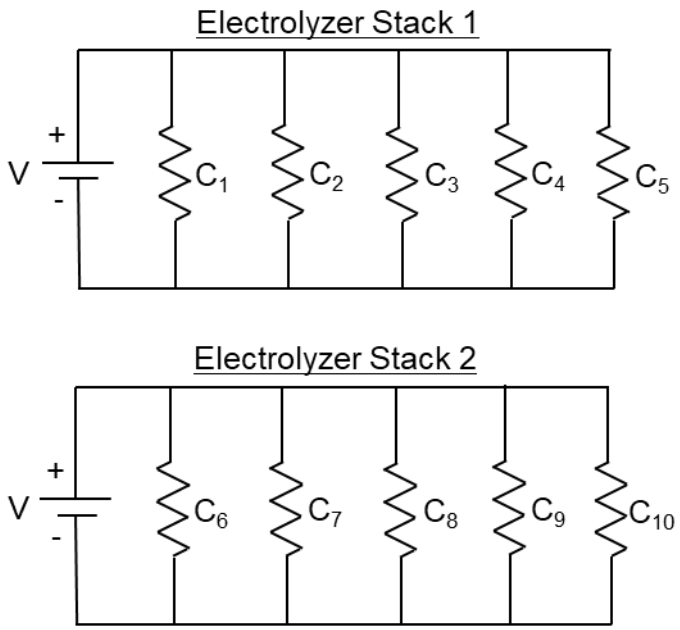

Figure S18. 10-cell (1,000 cm^2) electrolyzer stack electrical circuit configuration (C_x represents cell and the cell's respective number).

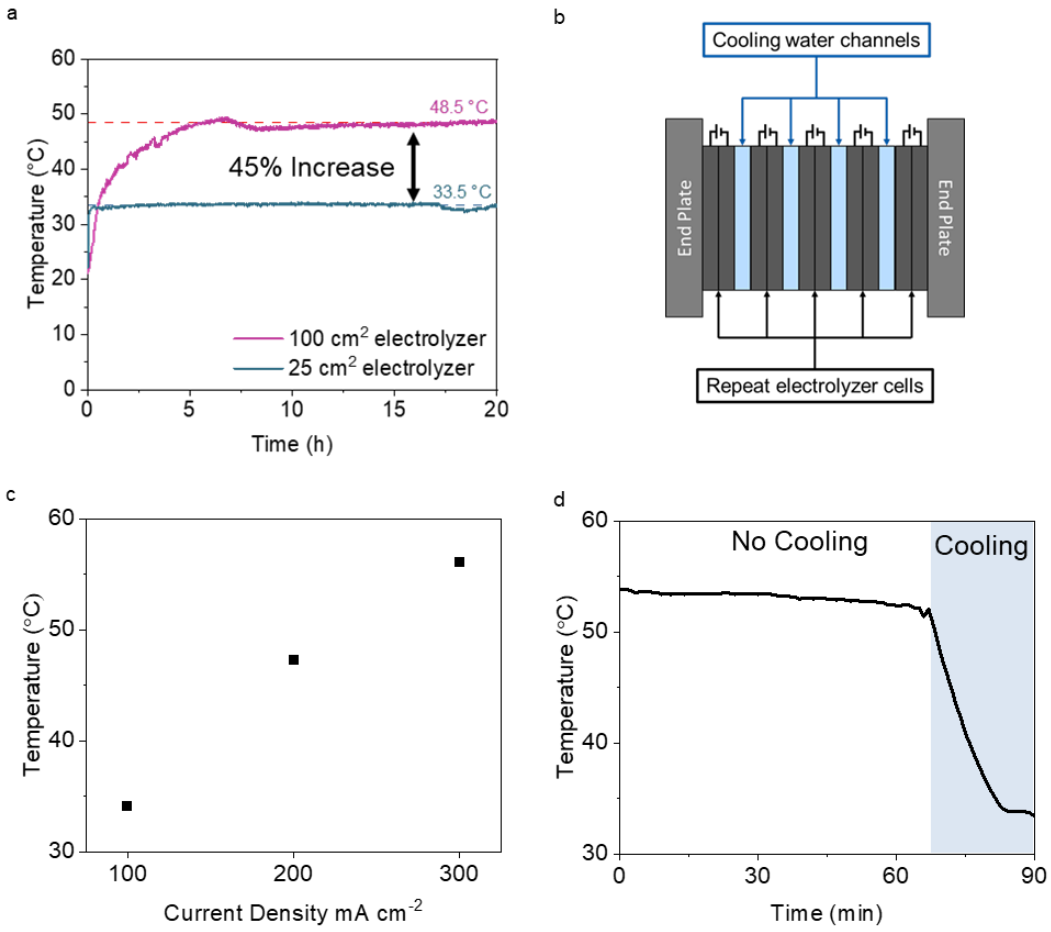

Figure S19. (a) Temperature over time for 5-cm^2 and 100-cm^2 active area without cooling, (b) schematic of cooling water channels in a 5 cell CO_2/CO electrolyzer stack, (c) temperature vs current density for 100 cm^2 electrolyzer cell, (d) impact of 35 °C cooling water fed to single 100-cm^2 electrolyzer cell. 2 M KOH, FAA-3-50, and NiFe anode were used.

Figure S20. Barrel of electrosynthesized acetate produced during stability testing (~1.2 M, >96% molar purity).

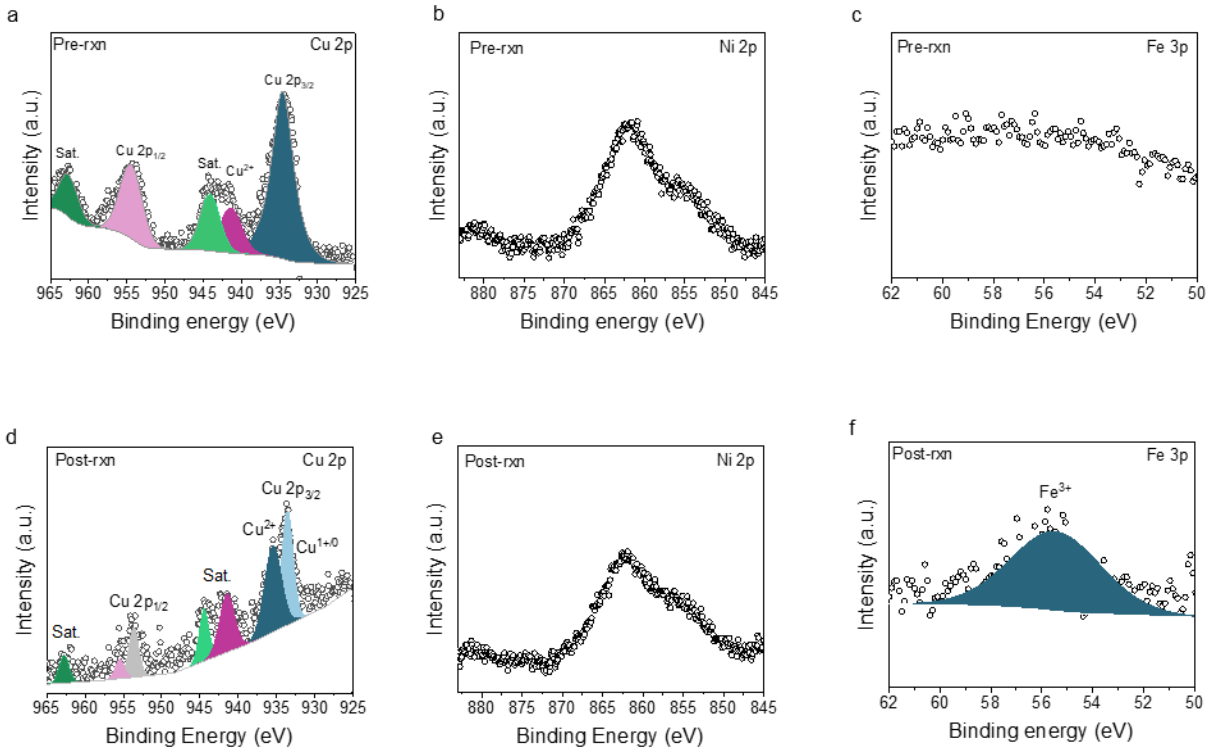

Figure S21. XPS measurements of 100-cm^2 Cu cathodes. Pre-reaction cathodes (a) Cu 2p, (b) Ni 2p, (c) Fe 3p and post-reaction cathodes (d) Cu 2p, (e) Ni 2p, (f) Fe 3p. Post-reaction cathodes were obtained after 125+ h in 1,00- cm^2 Stack stability experiment shown in Fig. 3d.

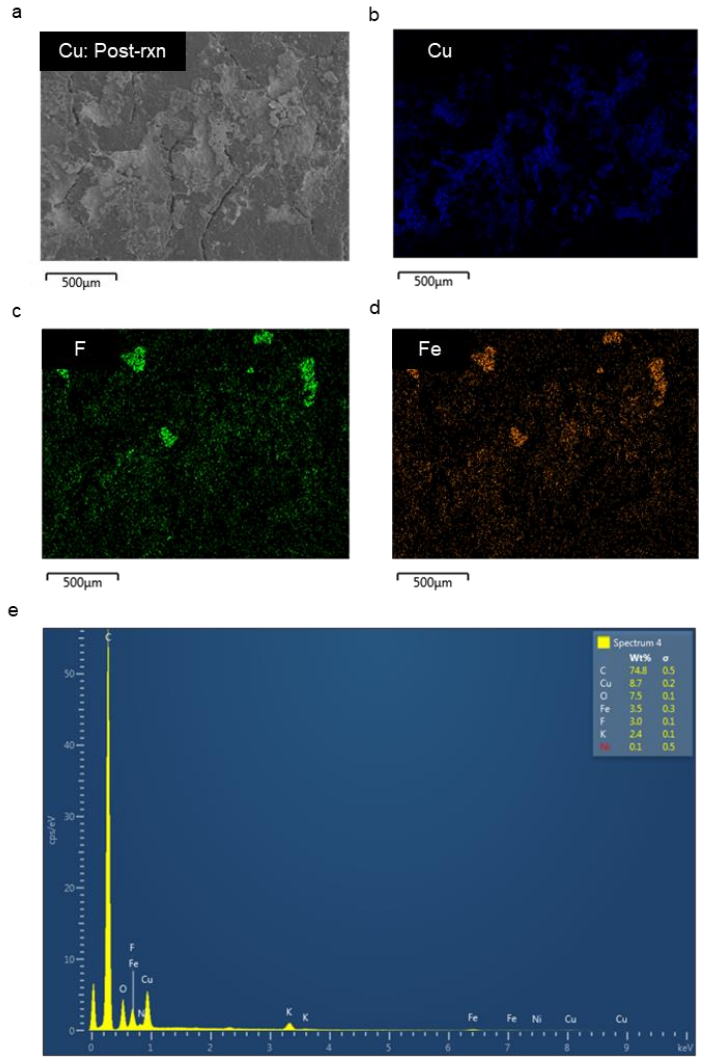

Figure S22. SEM-EDS images of post-reaction 100-cm^2 Cu cathodes. (a) SEM image of cathode (b) Cu elemental mapping (c) F elemental mapping (d) Fe elemental mapping (e) quantification of bulk elements. Post-reaction cathodes were obtained after 125+ h in 1,000-cm^2 Stack stability experiment shown in Fig. 3d.

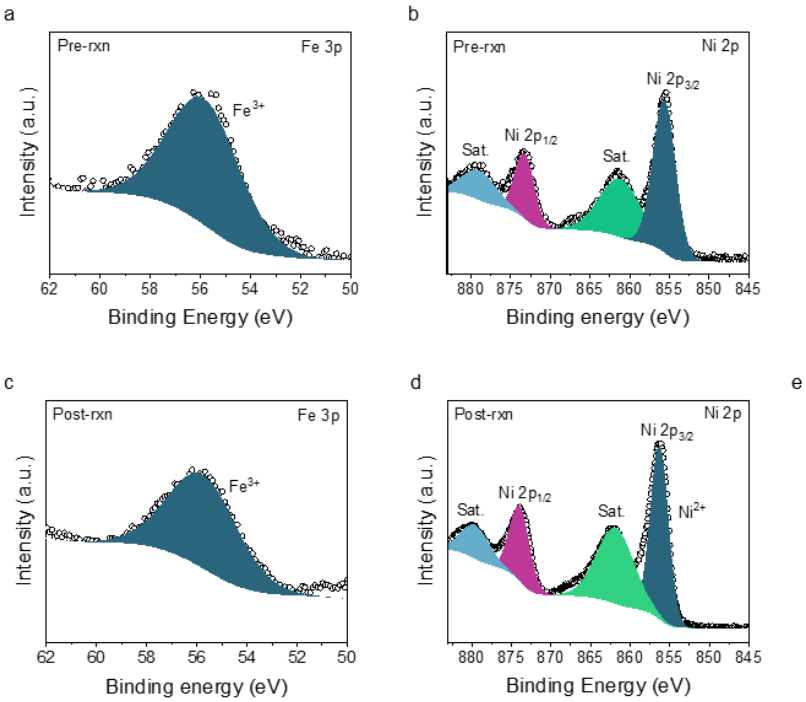

e

	Ni (atom. %)	Fe (atom. %)
Pre-rxn	48.4	51.6
Post-rxn	52.0	48.0

Figure S23. XPS measurements of 100-cm^2 Ni-Fe on Ni foam anodes. Pre-reaction anodes (a) Fe 3p, (b) Ni 2p and post-reaction anodes (c) Fe 3p, (d) Ni 2p. (e) Table of Ni and Fe ratio obtained from XPS measurements. Post-reaction anodes were obtained after 125+ h in 1,000-cm^2 Stack stability experiment shown in Fig. 3d.

a

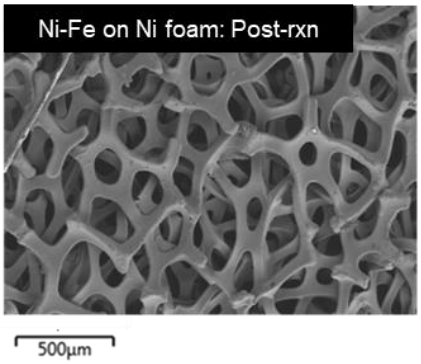

b

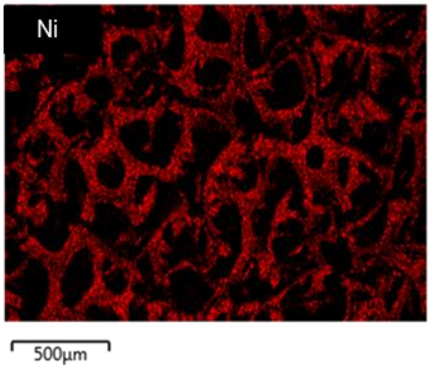

c

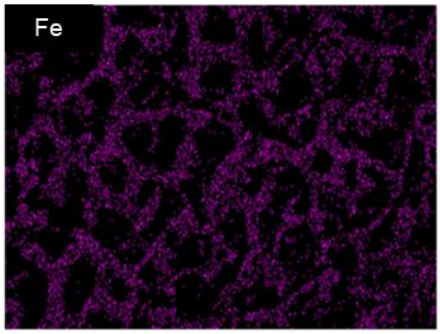

d

	Ni (atom. %)	Fe (atom. %)
Pre-rxn	86.8	13.2
Post-rxn	71.5	4.0

e

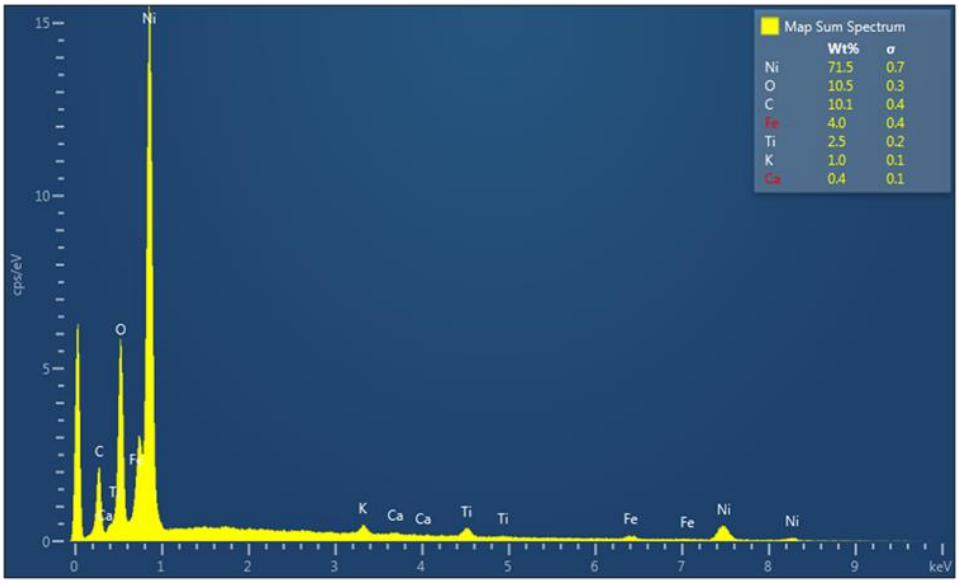

Figure S24. SEM-EDS images of post-reaction 100-cm^2 Ni-Fe on Ni foam anodes. (a) SEM image of anode (b) Ni elemental mapping (c) Fe elemental mapping (d) table of Ni and Fe ratio obtained from EDS measurements (e) quantification of bulk elements. Post-reaction anodes were obtained after 125+ h in 1,000-cm^2 Stack stability experiment shown in Fig. 3d.

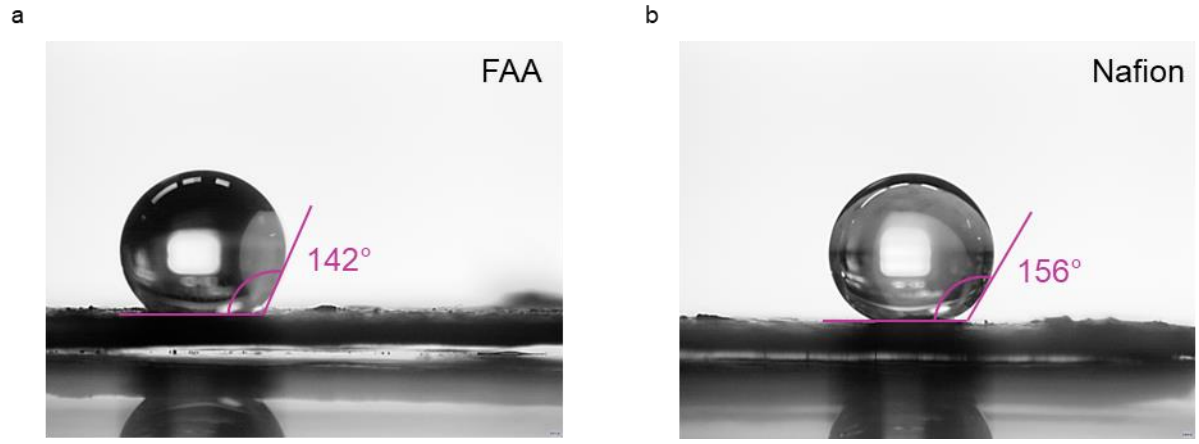

Figure S25. Contact angle measurements. (a) Cu on Sigracet 39BB carbon paper with 10 wt% Fumion FAA-3 ionomer and 10 wt% carbon black (b) Cu on Sigracet 39BB carbon paper with 10 wt% Nafion ionomer and 10 wt% carbon black.

Table S1. Comparison of two-step tandem CO_2 electrolysis stability from reported studies. SOEC and MEA refers to solid oxide electrochemical cell and membrane electrode assembly, respectively.

CO_2RR electrolyzer configuration	CORR electrolyzer configuration	CO_2RR current density (mA cm^{-2})	CORR current density (mA cm^{-2})	Two -step process operation time (h)	Reference
Room temperature electrolyzer (H-type cell)	Room temperature electrolyzer (H-type cell)	2	1	<1	[2]
Room temperature electrolyzer (3-compartment)	Room temperature electrolyzer (3-compartment)	100	200	<3	[3]
SOEC (800 ℃)	Room temperature electrolyzer (MEA)	550	120	40	[4]
Room temperature electrolyzer (MEA)	**Room temperature electrolyzer (MEA)**	**100**	**100**	**200**	**This work**

Table S2. Experimentally observed parameters used in techno-economic analysis.

Parameter	Value
Cell Voltage	2.26 V
Faradaic Efficiency	37%
Current Density	300 mA cm^{-2}
Cathode Catalyst	1 mg Cu cm^{-2}
*Copper Cost	1.18 USD kg^{-1}
Anode Catalyst	2 mg Ni cm^{-2} / 1 mg Fe cm^{-2}
*Nickel Cost	2.49 USD kg^{-1}
*Iron Cost	0.07 USD kg^{-1}

*Catalyst costs are based upon 5-year average bulk metal costs from 2015-2019[5]

Table S3. Techno-economic analysis major assumptions

Parameter	Value	Source
Plant Production Scale	50,000 kg day^{-1}	[6]
Plant Lifetime	20 years	[6]
Income Tax Rate	38.9%	[6]
Nominal Interest Rate	3.7%	[7]
Balance of Plant	61% of electrolyzer capital cost	[6]
Maintenance Cost	2.5% of electrolyzer capital cost	[8]
Material Replacement Cost	40% of electrolyzer capital cost	[8]
Plant Lifetime	20 years	[6]
Plant Operating Time	330 days $year^{-1}$	[9]
*Electricity Price	\$0.033 USD kWh^{-1}	[10]

*Electricity price based upon the global weighted average levelized cost of energy for onshore wind electricity production[8]

Table S4. Solid oxide electrolysis cell techno-economic parameters

Parameter	Value	Source
Energy Usage	6 kWh Nm^{-3}_{CO}	[11]
Power Usage	13 kW m^{-2}	[12]
CAPEX	1,250 USD kW^{-1}	[12]
Current Density	850 mA cm^{-2}	[12]
Cell Voltage	1.5 V	[12]
CO_2 Cost	35 USD ton^{-1}	[13]

Table S5. Techno-economic analysis cost breakdown (baseline scenario)

Cost Source	Contribution to Total Cost (%)
Power Usage	46.8%
Maintenance	0.7%
Stack Hardware	1.6%
Membrane	0.4%
Catalyst	0.2%
CO Production	28.4%
Water	0.2%
Distillation	8.2%
Electrolyte Recovery/Protonation	12.7%
Balance of Plant	0.9%

*Does not add up to 100.0% due to rounding

Supplementary References

1. Overa, S., et. al. Enhancing acetate selectivity by coupling anodic oxidation to carbon monoxide electroreduction. *Nat. Catal*. **5**, 738-745 (2022).

2. Theaker, N. *et al.* Heterogeneously catalyzed two-step tandem cascade electrochemical reduction of CO_2 to ethanol. *Electrochim. Acta* **274**, 1–8 (2018).

3. Cuellar, N. S. R., Scherer, C. & Ka, B. Two-step tandem electrochemical reduction of CO_2 towards multi-carbon products at high current densities. *J. CO_2 Util.* **36**, 263–275 (2019).

4. Ozden, A. *et al.* CO_2 electrolysis enables efficient carbonate-free production of ethylene. *Joule* **5**, 706-719 (2021).

5. Cradnall, B. S., Overa, S., Shin, H.. Jiao, F. Truning Carbon Dioxide into Sustainable Food and Chemicals: How Electrosynthesized Acetate is Paving the Way for Fermentation Innovation. *Acc. Chem. Res*. **56**, 1505-1506 (2023).

6. Shin, H., Hansen, K., Jiao, F. Techno-economic assessment of Low-Temperature Carbon Dioxide Electrolysis. *Nat. Sustain*. **4**, 911-919 (2021).

7. H2A: Hydrogen Analysis Production Models, Current Central Hydrogen Production from Polymer Electrolyte Membrane (PEM) Electrolysis (2019). version Nov 2020, National Renewable Energy Laboratory. https://www.nrel.gov/hydrogen/h2a-production-models.html

8. James, B., Colella, W., Moton, J. PEM Electrolysis H2A Production Case Study Documentation. (2013). https://www.nrel.gov/hydrogen/assets/pdfs/h2a-pem-electrolysis-case-study-documentation.pdf

9. Crandall, B. S., Brix, T., Weber, R. S., Jiao, F. Techno-Economic Assessment of Green H_2 Carrier Supply Chains. *Energy Fuels*. **37**, 1441-1450. (2023).

10. International Renewable Energy Agency. Renewable power generation costs in 2022. (2023). https://www.irena.org/Publications/2023/Aug/Renewable-Power-Generation-Costs-in-2022

11. TOPSOE. Produce Your Own Carbon Monoxide. https://www.topsoe.com/processes/carbon-monoxide

12. Ramdin, M. et al. Electroreduction of CO_2/CO to C_2 Products: Process Modeling, Downstream Separation, System Integration, and Economic Analysis. *Ind. Eng. Chem. Res*. **49**, 17862-17880 (2021).

13. International Energy Agency. Levelized Cost of CO_2 Capture by Sector and Initial CO_2 Concentration (2019). https://www.iea.org/data-and-statistics/charts/levelised-cost-of-co2-capture-by-sector-and-initial-co2-concentration-2019